Electronic Transport Studies of Bulk GaInP and AlGaInP Based on an Ensemble Monte Carlo Calculation Including Three-valley Band Structure Model

H. Arabshahi[1*] and M. R. Khalvati[2]
[1]*Physics Department, Ferdowsi University of Mashhad, Mashhad, Iran*
[2]*Physics Department, Shahrood University of Technology, Shahrood, Iran,*

An ensemble Monte Carlo simulation has been used to model bulk electron transport at room and higher temperatures as a function of high electric fields in GaInP and AlGaInP materials. Electronic states within the conduction band valleys at the Γ, *X* and *L* are represented by non-parabolic ellipsoidal valleys centered on important symmetry points of the Brillouin zone. The simulation shows that inter-valley electron transfer plays a dominant role in GaInP in high electric fields leading to a strongly inverted electron distribution and to a large negative differential conductance. Our simulation results have also shown that the electron velocity in AlGaInP is less sensitive to temperature than in GaInP. So, AlGaInP devices are expected be more tolerant to self-heating and high ambient temperature device modeling. Our steady state velocity-field characteristics are in fair agreement with other recent calculations.

1. Introduction

The quaternary alloy AlGaInP lattice matched to AlP shows promise as a suitable material for microwave devices such as field-effect transistors and Gunn diodes and for optoelectronic devices with tailored spectral response. As an aid to the device related work, the transport coefficients of the material need careful investigation. Therefore, the electron Hall mobility in the quaternary alloy has been measured [1-4] and Monte Carlo calculations of the mobility have also been performed [5-7]. In the mean time, our knowledge of the basic parameters and of the scattering mechanisms for the alloy has improved. Particularly, it is now known that the polar optic-phonon scattering, which is the dominant lattice scattering mechanism in the quaternary alloy, has a two-mode character [8]. It is important to calculate the transport coefficients using currently available information on scattering mechanisms and material parameters. We use such information in the present paper to calculate electron drift velocity in the quaternary alloy. We consider band non-parabolicity, admixture of p-type valance-band wave functions, degeneracy of the electron distribution to any arbitrary degree, and the screening effects of free carriers on the scattering probabilities. All the relevant scattering mechanisms, including the two-mode nature of the polar optic phonon scattering, are taken into account. Our calculated results are compared with the available experimental data on both the temperature and the composition dependence of mobility.

This article is organized as follows. Details of the conduction band parameters and the Monte Carlo simulation are presented in Sec. 2, the steady state simulation results are interpreted in Sec. 3, and conclusions are in Sec. 4.

2. Electronic structure, scattering and simulation models

Electronic transport is studied using the ensemble Monte Carlo simulation. The band structures of the materials under study are approximated with an analytical formulation using the non-parabolic spherical valleys. Though usage of an analytical band structure is questionable at high applied electric field strengths wherein impact ionization can occur, we adopt its usage here for the following reasons. First, due to the large number of compositions examined, it is too computationally expensive to utilize full band models with their concomitant numerically derived scattering mechanisms. Second, we have found that the analytical model reflects well the low field dynamics critical for assessing the carrier mobility. Since we restrict our work here only to low field phenomena, an analytical band structure is satisfactory. For each material, three nonequivalent valleys have been included. The primary valley for two materials occurs at Γ. The secondary minima included in the simulation are located at *L* and *X*. It

*arabshahi@um.ac.ir

should be noted that their relative energy ordering varies among the materials studied. In our Monte Carlo simulation, the four equivalent *L* valleys and the three equivalent *X* valleys, are represented by ellipsoidal, non-parabolic dispersion relationships of the following form [9-11]

$$E(k)\left[1+\alpha_i E(k)\right]=\frac{\hbar^2}{2}\left[\frac{k_x^2+k_y^2}{m_\perp^*}+\frac{k_z^2}{m_\parallel^*}\right] \qquad (1)$$

Where, $m^*_\perp$ and $m^*_\parallel$ are the transverse and longitudinal effective masses at the band edge and α_i is the non-parabolicity coefficient of i-th valley. The band structures of the quaternary compounds are determined from the binaries using the virtual crystal approximation. The non-parabolicity factors, effective masses and the inter-valley energy separations for binary compounds materials have been reported in [12-15]. The scattering mechanisms included within the simulation are: acoustic phonon scattering, the equivalent and nonequivalent inter-valley non-polar optical phonon scattering, polar optical phonon scattering, ionized impurity scattering, piezoelectric scattering, and alloy scattering [16-18]. The scattering parameters for the quaternary alloys are determined using linear interpolation. In the case of alloy scattering, the scattering rate is given as

$$R_{alloy}(k)=\frac{4\sqrt{2}\pi m^{*3/2}r_0^6}{9\hbar^4}\frac{x(1-x)(\Delta U)^2}{\Omega^2}\gamma^{1/2}(E)(1+2\alpha E) \qquad (2)$$

Where, *x* denotes the molar fraction of one of the binary components of the alloy, **Ω** is the volume of the primitive cell and ΔU is the spherical scattering potential. Different interpretations for the choice of random alloy potential have been given in the past. Littlejohn et al. [13] have used the conduction band offset to represent the random scattering potential.

3. Calculated results

Fig. 1 shows the simulated velocity-field characteristics of GaInP and AlGaInP at 300 K, with a background doping concentration of 10^{16}cm^{-3}, and with the electric field applied along one of the cubic axes. In this figure, the solid circle represent simulation results obtained for GaInP and the open circle curves are results obtained for AlGaInP. These simulations suggest that the peak drift velocity for zincblende GaInP and AlGaInP is about 0.9×10^5 ms^{-1}, whereas that for AlGaInP has no breakdown effect. At higher electric fields, inter-valley optical phonon emission dominates and causes the drift velocity to saturate at around 0.3×10^5 ms^{-1} for GaInP. The calculated drift velocities apparent from Fig. 1 are fractionally lower than those that have been calculated with assuming an effective mass in the upper valleys equal to the free electron mass. The threshold field for the onset of significant scattering into satellite conduction band valleys is a function of the inter-valley separation and the density of electronic states in the satellite valleys.

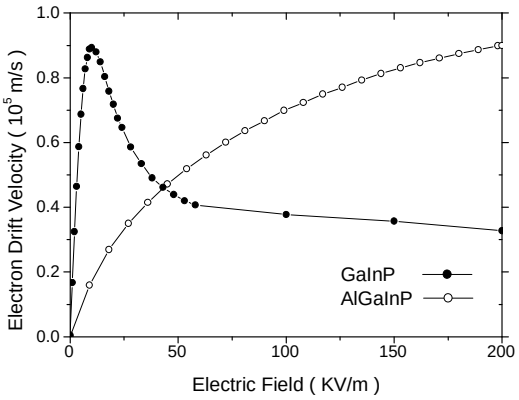

Fig.1: Calculated steady-state electron drift velocity in bulk zincblende GaInP and AlGaInP at room temperature with a background doping concentration of 10^{16}cm^{-3}.

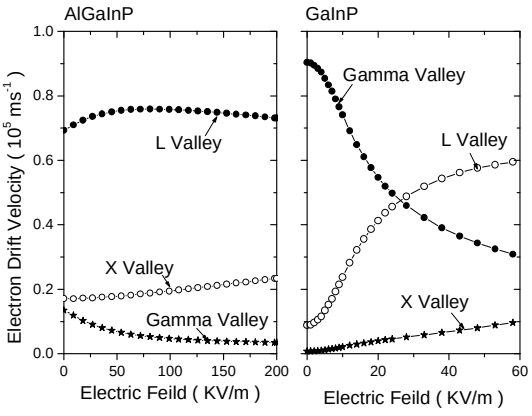

Fig.2: Fractional occupation of the central Γ and satellite valleys of zincblende GaInP and AlGaInP as a function of applied electric field using the non-parabolic band model at room temperature.

From Fig. 2, which shows the fractional occupancy of the available valleys as a function of applied field, the threshold fields are found to be 10^7 Vm^{-1} for zincblende GaInP and 2×10^7 Vm^{-1} for AlGaInP.

The average carrier kinetic energy as a function of electric field is shown in Fig. 3 for lattice temperature up to 500 K. These curves have the S shape typical of III-V compounds, which is a consequence of inter-valley transfer. At high fields, the curve for GaInP suggests that the average electron energy is higher than for AlGaInP. This difference can be understood by considering the Γ valley occupancy as a function of field (Fig. 5).

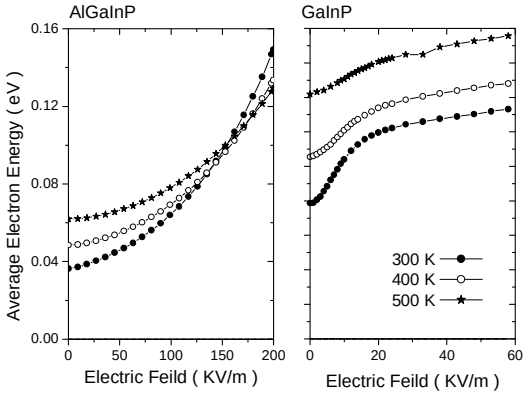

Fig.3: Average electron kinetic energy as a function of applied electric field in bulk GaInP and AlGaInP using the non-parabolic band model at different temperatures.

Inter-valley transfer is substantially larger in the GaInP than AlGaInP phase due to the combined effect of a lower Γ-valley effective mass, lower satellite valley separation and reduced phonon scattering rate within the Γ-valley, and a significant inter-valley phonon scattering at a threshold field of 1.5×10^{7} Vm^{-1}.

Fig. 3 shows the calculated electron drift velocity as a function of electric field strength for temperatures of 300, 450 and 600 K. The decrease in drift mobility with temperature at low fields is due to the increased intra-valley polar optical phonon scattering, whereas the decrease in velocity at higher fields is due to the increased intra and inter-valley scattering. It can also be seen from the figure that the peak velocity also decreases and moves to higher electric field as the temperature is increased. This is due to the general increase of total scattering rate with temperature, which suppresses the electron energy and reduces the population of the satellite valleys. This latter effect is apparent from the fact that the electron population in the Γ-valley increases with temperature as shown in Fig. 4.

Fig. 4 shows how the velocity-field characteristic of GaInP and AlGaInP changes with the impurity concentration at 300 K. It is clear that with an increasing donor concentration there are small changes in the average peak drift velocity and the threshold field (Fig. 6). These results show the trend expected from increased ionized impurity scattering is in good agreement with recent calculations performed by other workers [19].

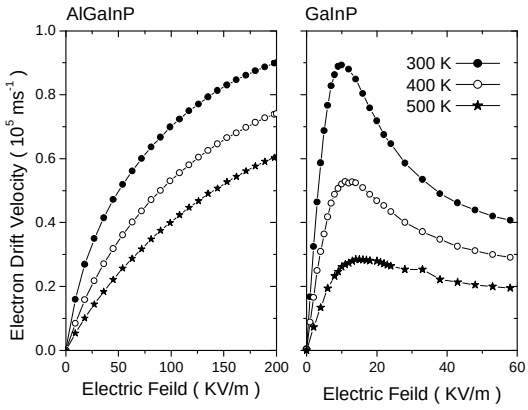

Fig.4: Calculated electron steady-state drift velocity in bulk GaInP and AlGaInP as a function of applied electric field at various lattice temperatures and assuming a donor concentration of 10^{22} m^{-3}. The peak drift velocity decreases by about 20%, while the threshold field increases by same percent as the lattice temperature increases from 300 to 600 K.

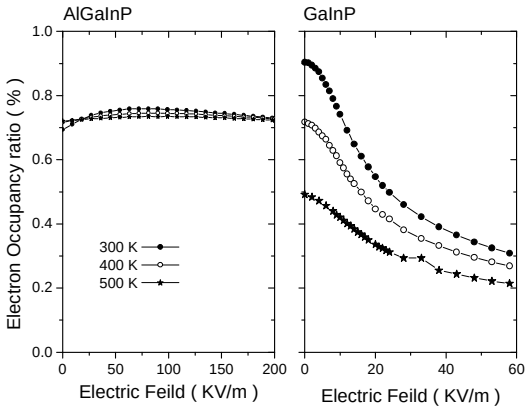

Fig.5: Central Γ valley occupancy as a function of applied electric field in bulk GaInP and AlGaInP using the non-parabolic band model at different temperatures.

4. Conclusions

Electron transport at different temperatures in bulk GaInP and AlGaInP have been simulated using an ensemble Monte Carlo simulation method. Using valley models to describe the electronic band structure, calculated velocity-field characteristics show that the inter-valley transitions in high electric fields play an important role in GaInP,

despite a large separation between the central and upper valleys. The inter-valley transitions lead to a large negative differential conductance. Saturation drift velocities of about 0.3×10^5 ms^{-1} match recent measurements on low-doped bulk samples. We have also demonstrated that low temperature sensitivity of the electron transport properties of wurtzite AlGaInP is attractive for high temperature and high power electronic applications.

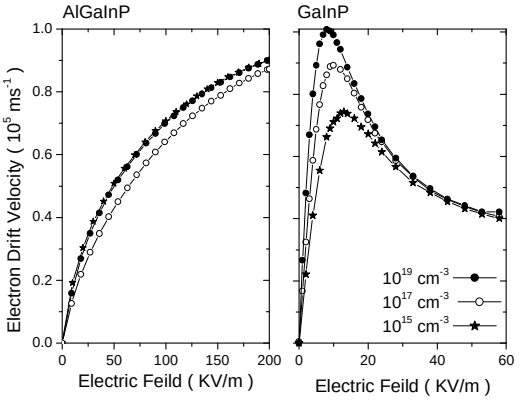

Fig.6: Electric field dependence of the drift velocity in GaInP and AlGaInP at 300 K for various donor concentrations.

Acknowledgments

I would like to thank M. G. Paezi for her useful comments.

References

[1] S. Nakamura, M. Senoh and T. Mukai, Appl. Phys. Lett. **62**, 2390 (1993).
[2] K. F. Lognbach and W. I. Wang, Appl. Phys. Lett. **59**, 2427 (1991).
[3] H. Kitabayashi, T. Waho and M. Yamamoto, Appl. Phys. Lett. **71**, 512 (1997)
[4] D. H. Chow, R. H. Milnes, T. C. Hasebberg, A. R. Kost, Y. H. Zhang and L. West, Appl. Phys. Lett. **67**, 3700 (1995).
[5] J. Johnson, L. A. Samoska, A. C. Gossard and S. M. Johnson, J. Appl. Phys. **80**, 1116 (1996).
[6] H. Mohseni, E. Michel, J. Sandoen and G. Brown, Appl. Phys. Lett. **71**, 1403 (1997).
[7] J. R. Meyer, C. A. Hoffman, F. J. Bartoli and L. R. Ram-Mohan, Appl. Phys. Lett. **67**, 2756 (1995).
[8] S. Strite and H. Morkoc, J. Vac. Sci. Technol. **B 10**, 1237 (1992).
[9] C. Moglestue, *Monte Carlo Simulations of Semiconductor Devices* (Chapman and Hall, 1993).
[10] C. Jacoboni and P. Lugli, *The Monte Carlo Method for Semiconductor and Device Simulation* (Springer-Verlag, 1989).
[11] U. V. Bhapkar and M. S. Shur, J. Appl. Phys. **82**, 1649 (1997).
[12] J. Kolnik, I. H. Oguzman and K. F. Brenan, J. Appl. Phys. **81**, 726 (1997).
[13] M. A. Litteljohn, J. R. Hauser and T. H. Glisson, Appl. Phys. Lett. **83**, 625 (1975).
[14] K. F. Brennan, D. H. Park, K. Hess and M. A. Littlejohn, J. Appl. Phys. **63**, 5004 (1988).
[15] N. S. Mansour, K. Diff and K. F. Brennan, J. Appl. Phys. **70**, 6854 (1991).
[16] J. Kolnik, I. H. Oguzman and K. F. Brennan, J. Appl. Phys. **78**, 1033 (1995).
[17] B. E. Foutz, L. F. Eastman, U. V. Bhapkar and M. Shur, Appl. Phys. Lett. **70**, 2849 (1998).
[18] J. D. Albrecht, R. P. Wang and P. P. Ruden, J. Appl. Phys. **83**, 2185 (1998).
[19] B. E. Foutz, S. K. O'Leary, M. S. Shur and L. F. Eastman, J. Appl. Phys. **85**, 7727 (1999).

Received: 1 March, 2009
Revised: 27 July, 2009
Accepted: 4 August, 2009